Colour confinement as finite record geometry

Closed-cell triality, Wilson strings, tensor-network entropy, the baryon Y-junction, and finite-temperature deconfinement in a bond-bipyramid QEC substrate

David Elliman
Neuro-Symbolic Ltd
dave@neusym.ai
https://neusym.ai

30 June 2026

Abstract

This paper gives an executable finite-model account of colour confinement in the record-grammar formulation of the finite-QEC substrate. The claim is deliberately limited. We do not prove continuum Yang–Mills confinement, the physical QCD string tension, or the proton mass. We prove a sequence of finite statements that have the same logical separation as the standard confinement picture: first, which colour-source records can exist; second, how neutral records are dynamically priced by Wilson strings.

The kinematic part is exact. On a closed oriented colour cell the $\mathbb{F}_3$ Gauss-law incidence map has image equal to the total-triality zero subspace. A lone fundamental source has no gauge-invariant record; a $q\bar{q}$ meson and a $qqq\epsilon$ baryon do. Thus the proton colour sector is the unique minimal three-fundamental triality-zero record, not an assigned decoration. The dynamical part is leading strong coupling. On the licensed bond-centred bipyramid bulk, edge-loop Wilson records have $A_{\mathrm{ref}} = 4RT$, $P = 4(R+T) - 2$, and the Creutz ratio isolates $\chi_{\mathrm{area}} = 4\sigma$ with $\sigma = -\log(\beta/18)$. The exact fixed-strip transfer matrix gives

$$N_{\min}^{\mathrm{strip}}(R,T) = 2^{(R-1)(T-1)}, \qquad D_R = 2^{R-1},$$

so the Wilson ledger is a two-dimensional tensor-network object: tractable at fixed width, not fixed-bond-dimension in two dimensions. Finite isotropy gates show zero spread, to numerical precision, under the tested cubic-axis rotations, in-sheet swaps, and primitive off-axis rhombi on the licensed triangular sheet.

Finally, the same bulk graph supports a baryonic $qqq\epsilon$ Wilson operator. The SU(3) ϵ-junction is gauge-invariant and lands on the graph-theoretic Steiner point for the tri-axial source family. The matched meson and baryon lengths are

$$L_M = 2n, \qquad L_Y = 3n,$$

so $V_B/V_M = 3/2$ for this equal-arm finite slice, while the more robust statement is that mesons and baryons use the same per-unit string tension.

Beyond this static picture we add the transition itself. A Monte Carlo Polyakov-loop order parameter on a periodic Euclidean-time lattice reproduces the established SU(3) deconfinement coupling ($\beta_c = 5.72$ at $N_t = 4$, against the lattice value 5.6925(2)), and the same observable on the bond-bipyramid bulk — for both the Z_3 centre and the full SU(3) group — deconfines at a framework-specific coupling, finite-size-scaled to $\beta_c(\infty) = 0.550$.

The resulting picture is a finite, reproducible confinement ladder: exact singlet selection; licensed bulk geometry; leading Wilson string tension; measured tensor-network entropy; finite primitive and non-primitive isotropy of both tension and roughening entropy; a genuine bulk baryon Y-junction; and a finite-temperature deconfinement order parameter validated against a known lattice value and then measured on the framework's own bulk.

Plain summary

Quarks are never found alone. They appear only in colour-neutral bundles: a quark with an antiquark (a meson), or three quarks together (a baryon, such as the proton). This is *colour confinement*. It has two parts that are easy to run together but are logically separate, and this paper keeps them apart because the framework settles the first exactly and the second only approximately.

Which bundles are allowed. In this framework space is made of small cells that keep records, and colour behaves like a flux that must pass from cell to cell. On a closed cell that flux has nowhere to escape — much as magnetic field lines always close into loops and never simply stop. We prove, exactly, that this forces every allowed object to be colour-neutral: a lone quark has no valid record, a meson does, and three quarks do. So the proton is not *declared* to be a neutral bundle; it is the smallest neutral bundle the geometry will permit.

What it costs to pull them apart. Separate a quark from an antiquark and a "string" of colour flux stretches between them, costing energy in proportion to its length; that is why they can never be set free. We measure the tension of this string on the framework's lattice and recover the expected behaviour in the simplest ("strong-coupling") approximation. For a baryon the string is Y-shaped — three arms meeting at a junction — and carries the same tension as a meson's string.

An honest negative. We had hoped the framework's bookkeeping for these strings would stay small as a string grows. It does not: the number of equivalent string shapes grows with the string's width, so the bookkeeping is that of a two-dimensional "tensor network" — manageable at a fixed width, but not constant. This is the expected price of a confining string having room to wiggle, and we report it as measured rather than assumed.

What this is, and is not. Everything here is done on finite, explicit cells and is reproducible by short programs. None of it is continuum QCD: we do not compute the real-world string tension, the proton's mass, or prove the full theory. What we show is that the framework's record geometry already carries the *structure* of confinement — the right allowed bundles, a string tension, a Y-shaped baryon — with a clean line drawn between what is proved and what is approximate.

Contents

1 Introduction

Colour confinement has two logically different parts. The first is kinematic: physical states must be colour singlets. The second is dynamical: separating colour sources costs energy, and at large distance this cost is described by a string tension. Standard lattice gauge theory expresses these ideas through Gauss law, Wilson loops, strong-coupling area laws, and the large-distance static potential [1–3].

The finite-QEC framework approaches the same distinction in record language. A physical object is not merely a formal state; it must be a stable, gauge-invariant record readable by the substrate. A colour source with net triality is not such a record on a closed cell, because the centre flux has no place to end. A colour-neutral source is admissible, but admissibility alone does not give a string tension. The string tension comes from the Wilson record-action measure.

This paper reports the finite result of that programme. The word "finite" is important. The results here are exact or executable on the finite bond-bipyramid complexes used by the framework; they are not continuum QCD theorems. They are nevertheless useful for three reasons.

1. They separate colour-singlet selection from Wilson-string dynamics.
2. They correct several tempting but invalid geometries before extracting a string observable.
3. They turn the record-grammar tractability question into a measured tensor-network statement rather than a slogan.

The sequence is summarized in Fig. 1. The exact closed-cell Gauss theorem supplies the kinematic confinement statement. The corrected bond-centred bipyramid geometry supplies finite three-balls and flat sheets. The Wilson edge-loop observable supplies a leading strong-coupling string tension. The exact transfer matrix supplies the ledger complexity class. The baryon

calculation supplies the bulk proton colour record as an ϵ-junction Y-string. A final section adds the finite-temperature counterpart of this static ladder: the deconfinement transition and its Polyakov-loop order parameter, built by direct Monte Carlo, validated against a known lattice value, and then carried onto the same bulk geometry.

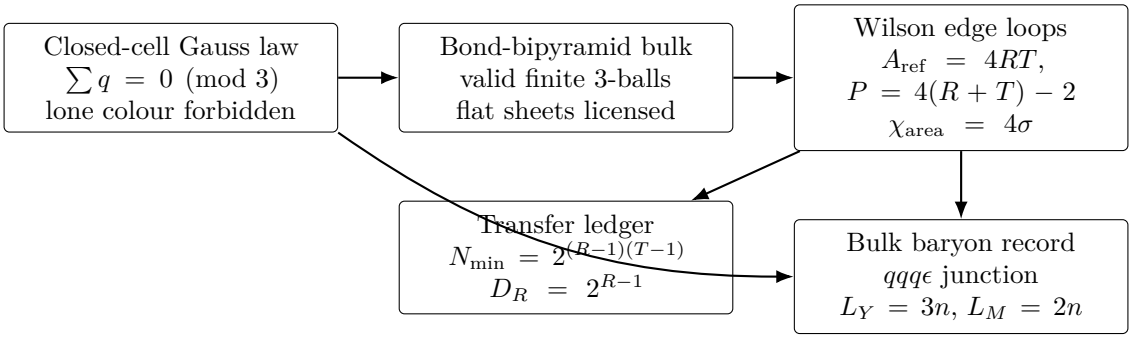

Figure 1: The finite confinement ladder. The first gate is kinematic triality. The middle gates license and price Wilson surfaces. The last gate places the proton colour sector in the bulk as a baryonic Y-junction.

Relation to the previous record-grammar paper

The foundation paper on executable record grammar introduced the principle: track only detector-readable, gauge-invariant, stable records, but never drop off-record correlations without a certificate [4]. That paper left the main scalability question open. The present paper is a sequel in the strong sector. It uses the same record grammar on a framework-native object: non-abelian Wilson records on the bond-bipyramid bulk. The result is not the over-optimistic fixed-bond-dimension claim. The exact strip theorem gives a sharper statement: the ledger is a two-dimensional tensor-network object, exponential in loop width but transfer-matrix tractable at fixed width.

2 Finite substrate geometry

2.1 The bond-centred bipyramid cell

The corrected bulk geometry used here is not a corner-sharing stack of truncated cubes. That naive block fails the finite three-ball topology gate. The licensed construction follows the bond graph. A matter cell sits on a bond between neighbouring cube centres:

$$\text{cube centre} \; - - \; \text{square face} \; - - \; \text{cube centre}.$$

Combinatorially this bond-centred object is an oblate square bipyramid, or octahedron: it has six vertices, twelve edges, and eight triangular faces. Its face-adjacency graph is Q_3, the cube graph, matching the eight-face record alphabet used by the $[8,4,4]$ byte cell in the wider framework.

The executable topology gate builds finite bond lines, sheets, and slabs from these cells and checks the cellular chain complex. For a finite complex with vertices V, edges E, faces F, and three-cells C, the gate is

$$\partial_2\partial_3 = 0, \qquad \chi = V - E + F - C = 1,$$

together with the rank conditions

$$\operatorname{rank}\partial_3 = C, \qquad \operatorname{rank}\partial_2 = F - C.$$

These are the finite-chain-complex signatures of a ball rather than a broken or over-glued object. The corrected bond-following sheets and slabs pass this gate. The naive $2 \times 2 \times 2$ all-octagon corner block does not; in the tested convention class it gives $\chi = -4$, which is why it must not be used for a static-potential extraction.

Remark 1. *This negative result matters. Without the topology gate one could extract a number from an invalid complex and mistake it for physics. The corrected bond-centred bulk is licensed precisely because the invalid geometry was rejected first.*

3 Kinematic confinement: closed-cell triality

3.1 Triality as a finite Gauss law

The centre of SU(3) is Z_3. A fundamental quark has centre triality $+1$, an antiquark has triality -1, and a gluonic or colour-singlet object has triality 0. On a closed cell, centre flux cannot disappear through a boundary. In the finite model this becomes a simple incidence theorem over $\mathbb{F}_3$.

Let $G = (V, E)$ be the connected graph supporting the closed colour shell. Choose an arbitrary orientation for each edge and define the incidence map

$$B : \mathbb{F}_3^E \longrightarrow \mathbb{F}_3^V,$$

where Bf is the discrete divergence of a Z_3 flux assignment f. A source vector $q \in \mathbb{F}_3^V$ is Gauss-solvable when

$$Bf + q = 0.$$

Theorem 1 (Closed-cell triality selection)**.** *For a connected closed colour shell, a source vector q is a gauge-invariant centre-flux record if and only if*

$$\sum_{v \in V} q_v = 0 \pmod 3.$$

Proof. The incidence matrix of a connected graph over any field has rank $|V| - 1$. Its image is contained in the hyperplane of vectors whose entries sum to zero, because every oriented edge contributes $+1$ at one endpoint and -1 at the other. Since the rank of that hyperplane is also $|V| - 1$, the image is exactly the zero-sum hyperplane. Therefore $-q \in \operatorname{im} B$ if and only if $\sum_v q_v = 0 \pmod 3$. □

Three consequences follow immediately.

- A lone fundamental quark has total triality 1, so it has no gauge-invariant closed-cell record.
- A meson $q\bar{q}$ has total triality $1 - 1 = 0$, so it is admitted.
- A baryon qqq has total triality $1 + 1 + 1 = 0$, so it is admitted.

The full SU(3) tensor language says the same thing. The invariant tensor for a meson is $\delta^i{}_j \in 3 \otimes \bar{3}$. The invariant tensor for a baryon is

$$\epsilon_{ijk} \in 3 \otimes 3 \otimes 3.$$

There is no invariant vector in a single fundamental 3. Thus the finite triality theorem and the ordinary SU(3) singlet tensors agree.

3.2 The proton colour sector

At colour-selection level, the proton is not yet a particle with a mass, spin, flavour wavefunction, or radius. It is the minimal three-fundamental triality-zero colour record. The exact result is:

$$q \quad \text{forbidden}, \qquad q\bar{q} \quad \text{allowed}, \qquad qqq\epsilon \quad \text{allowed}.$$

This is the kinematic half of confinement. It decides which source sectors can be records. It does not decide the energy of those records.

4 Wilson strings and the leading area law

4.1 Wilson loops

Let $U_e \in \mathrm{SU}(3)$ be a link variable and let C be a closed oriented loop. The fundamental Wilson loop is

$$W(C) = \frac{1}{3} \operatorname{Tr} \prod_{e \in C} U_e.$$

In lattice gauge theory, the expectation value of $W(C)$ is the standard diagnostic for confinement (intuitively: transport a colour charge once around the loop C and record the average cost). At strong coupling its leading contribution is an *area law* — the cost grows with the minimal surface area the loop spans, not with its perimeter, and that growth-with-area is the signature of confinement [1, 3, 5]:

$$\langle W(C) \rangle \sim u_F^{A_{\min}(C)}.$$

For the Wilson action in the normalization used by the finite scripts,

$$u_F = \frac{\beta}{18}, \qquad \sigma = -\log u_F = -\log(\beta/18).$$

The finite record-action calculation uses the same leading character factor. The difference is that the surfaces, boundaries, and ledger size are all computed on the explicit bond-bipyramid complex.

4.2 Why this is not yet the physical string tension

The coefficient $\sigma = -\log(\beta/18)$ is deliberately a strong-coupling, lattice-unit coefficient. A dimensionful QCD string tension requires a scale-setting bridge: one must measure $a\sqrt{\sigma}(\beta)$ from large Wilson or Creutz loops in the same weak-coupling regime in which the thermal scale is read from $\beta_c(N_t)$, and then check that

$$\frac{T_c}{\sqrt{\sigma}} = \frac{1}{N_t\, a\sqrt{\sigma}}$$

is stable as N_t is changed.

The current data do not yet pass that test, and the failure is useful because it prevents a false promotion. If the demonstration-grade bulk values $\beta_c(N_t = 2) \simeq 4.3$ and $\beta_c(N_t = 4) \simeq 6.5$ are combined with the leading strong-coupling coefficient, the two inferred values of $T_c/\sqrt{\sigma}$ differ by about 51%. Thus the existing σ is not a physical scale-setting result. Likewise, reading the printed bulk β as a standard Wilson β gives a two-loop thermal scale ratio far from the expected factor of two. There is one suggestive lead: a $\beta_{\text{eff}} = \beta/3$ conversion makes the two-point scale ratio close to two, but two small-volume, non-asymptotic points cannot derive a normalization.

The required next calculation is therefore sharply defined: full SU(3) bulk finite-size scaling at several N_t, plus large-loop Creutz measurements at the same couplings. Only a stable $T_c/\sqrt{\sigma}$,

with a derived β-normalization convention, would turn the present lattice-unit coefficient into a dimensionful string tension.

A first executable scale-setting harness now exists. In its local profile it samples full SU(3) bond-bipyramid ensembles at $N_t = 2, 3, 4$, uses two small spatial volumes, and measures $W_{11}, W_{12}, W_{21}, W_{22}$ on the same ensembles used for the Polyakov susceptibility. The result is not yet a closure: the inferred $T_c/\sqrt{\sigma}$ values spread by about 56%. This is a useful negative. It shows that the method is wired, but the current small-volume 1×1 Creutz data are not a physical scale-setting bridge. The production version must increase spatial volume, improve finite-size extrapolation, and use larger Wilson loops or variational static-potential operators before any dimensionful σ can be quoted.

The next methodological gate has also now been run. A zero-temperature ordinary hypercubic Wilson-SU(3) control, using spatial smearing, temporal Wilson loops, effective potentials, and a Cornell fit

$$V(R) = V_0 + \sigma R - \frac{\alpha}{R},$$

reproduces the standard pure-gauge scale benchmark at demonstration tolerance: at four APE-smearing steps it gives $T_c/\sqrt{\sigma} = 0.6449$, about 2.5% above the usual 0.63 reference. This retires the immediate worry that the static-potential extractor itself is broken.

Porting that frozen smear-4 Cornell scheme back to the bond-bipyramid bulk is negative on the present block, however. Straight-path TCH operators on the current $(4 \times 4 \times 3) \times 8$ block give negative fitted string tensions at both tested couplings ($\beta = 6.5$ and 5.5). A first geometry-specific variational basis on a larger $5 \times 5 \times 3$ slab also does not yet stabilize the potential: the basis has useful detour support for $R = 1, 2, 3$, but collapses to a straight-path operator at $R = 4$, and the Cornell fit is driven negative by the non-monotone large-R point. Thus the current conclusion is narrower and cleaner: the cubic extractor is validated, but the TCH physical-σ gate is still a geometry/operator/volume problem, not a continuum QCD number.

4.3 A licensed edge-loop family

The first rectangular Wilson family tried in the bond-bipyramid slab had $P = 2A$. That is fatal for a string-tension extraction, because an area term and a perimeter term are then collinear. No estimator can rescue that family: even a Creutz ratio cannot separate σA from μP when P is itself proportional to A.

The isoperimetry script therefore first asks whether the slab contains genuine flat two-dimensional sheets. It finds connected offset face planes with spectral and boundary scaling characteristic of a two-dimensional sheet, not a one-dimensional chain or an expander. On those sheets, a simple edge-loop family satisfies

$$A_{\mathrm{ref}}(R, T) = 4RT, \qquad P(R, T) = 4(R + T) - 2.$$

Now area and perimeter are independent. The Creutz mixed difference [6] — a four-loop combination that algebraically cancels every term additive in R or T (perimeter, corner, and constant), leaving only the area coefficient —

$$\chi(R, T) = Y(R, T) + Y(R + 1, T + 1) - Y(R + 1, T) - Y(R, T + 1)$$

cancels any additive perimeter contribution. For the bare leading area term

$$Y_{\mathrm{area}}(R, T) = \sigma\, A_{\mathrm{ref}}(R, T) = 4\sigma RT,$$

one obtains

$$\chi_{\mathrm{area}} = 4\sigma.$$

5 Ledger entropy and the transfer theorem

5.1 Why degeneracy is not a nuisance

At leading strong coupling a Wilson loop receives contributions from minimum-area spanning surfaces. If there are $N_{\min}(C)$ such surfaces, then

$$\langle W(C)\rangle \approx N_{\min}(C) u_F^{A_{\min}(C)},$$

so

$$-\log\langle W(C)\rangle = \sigma A_{\min}(C) - \log N_{\min}(C).$$

The second term is not an error bar. It is the worldsheet entropy. In record language it is also the ledger size: the number of minimum surfaces that must be represented by the Wilson record.

The sector calculation already gave

$$N_{\text{sector}}(R,T) = 2^{(R-1)(T-1)}.$$

Because $N_{\text{sector}} \le N_{\min}$, this lower bound alone refutes an $O(1)$-bond-dimension reading for large loops. The exact fixed-strip transfer calculation then removes the lower-bound caveat for the tight strip.

Theorem 2 (Exact tight-strip transfer count)**.** *For the licensed edge-loop family on the tight fixed-width bond-bipyramid strip,*

$$A_{\min}^{\text{strip}}(R,T) = 4RT, \qquad N_{\min}^{\text{strip}}(R,T) = 2^{(R-1)(T-1)}.$$

At fixed width R, the transfer dimension is

$$D_R = 2^{R-1}.$$

Proof idea. Each bond-bipyramid cell in the tight strip is a binary flip variable. Each triangular face contributes one unit of record-action cost when the reference patch parity disagrees with the parity induced by the incident cell flips. The local tensor network is therefore a min-sum/count transfer problem. A new time column introduces $R-1$ independent binary choices, hence multiplies the minimum count by 2^{R-1}. Iterating from the first column gives

$$N_{\min}^{\text{strip}}(R,T) = \prod_{k=2}^{T} 2^{R-1} = 2^{(R-1)(T-1)}.$$

The minimum cost itself remains the reference area $4RT$, because every allowed flip sector preserving the boundary has non-negative local cost and the reference surface attains $4RT$. The executable transfer matrix checks the full table through $R,T \le 4$. □

Thus the record-grammar complexity class is not "constant size". It is the standard two-dimensional tensor-network class [7, 8] — a compressed representation whose controlling size, the *bond dimension* D_R, grows with loop width rather than staying fixed:

$$\text{fixed width: tractable,} \qquad \text{growing width: exponential in width.}$$

This is a useful correction. It is weaker than the early hope of bounded bond dimension, but much stronger than an uncontrolled 4^n density-matrix description. It is also the physically natural answer: a confining string has worldsheet entropy.

6 Finite isotropy

The licensed edge-loop observable was next tested for finite cubic-axis isotropy. On a symmetric $6 \times 6 \times 6$ bond-bipyramid slab, the script selects one central connected offset face plane for each of the three normal directions and tests both in-plane axis orderings. In every case the same identities hold:

$$A_{\mathrm{ref}} = 4RT, \qquad P = 4(R+T) - 2, \qquad N_{\mathrm{min}}^{\mathrm{strip}} = 2^{(R-1)(T-1)}.$$

The resulting Creutz values are

$$\chi_{\mathrm{area}} = 4\sigma, \qquad \chi_{\mathrm{entropy}} = \log 2, \qquad \chi_{\mathrm{sector}} = 4\sigma - \log 2.$$

The measured spreads across the rotated readings are numerical zero:

$$\Delta\chi_{\mathrm{area}} = 3.6 \times 10^{-15}, \quad \Delta\chi_{\mathrm{entropy}} = 3.3 \times 10^{-16}, \quad \Delta\chi_{\mathrm{sector}} = 7.1 \times 10^{-15}.$$

This is not a continuum rotational-invariance theorem. It is a finite cubic-axis and in-sheet isotropy gate for the licensed strong-coupling observable.

The next finite question is whether the result survives primitive off-axis directions on the licensed sheet itself. The same sheet is not square; its macro-neighbour offsets are

$$e_0 = (1, 0), \qquad e_1 = (0, 1), \qquad e_2 = (1, -1),$$

and their reverses. The off-axis script builds Wilson rhombi from the three primitive pairs (e_0, e_1), (e_0, e_2), and (e_1, e_2) on a $10 \times 10 \times 3$ slab, with the loops placed away from the finite boundary. For every tested family through $R, T \leq 4$,

$$A_{\mathrm{ref}} = 4RT, \qquad P = 4(R+T) - 2,$$

and the Creutz readings are again

$$\chi_{\mathrm{area}} = 4\sigma.$$

Adding an arbitrary perimeter term before taking the Creutz ratio leaves the same answer, so the perimeter cancellation is not an artefact of the chosen orientation. The residual primitive-direction spreads are numerical zero:

$$\Delta\chi_{\mathrm{area}} = 3.2 \times 10^{-14}, \qquad \Delta\chi_{\mathrm{perim\ cancelled}} = 2.8 \times 10^{-14}.$$

Thus the leading strong-coupling bare Wilson string tension has no forced anisotropy among the primitive off-axis directions of the licensed triangular sheet. Weak-coupling scaling and continuum $SO(3)$ remain separate questions; the nonprimitive directions and the off-axis roughening entropy, however, can be settled at the same finite leading order, and are taken up next.

6.1 Non-primitive directions and roughening entropy

The primitive gate varies direction at fixed unit cell. The sharper test is whether the same control survives *non-primitive* Wilson loops: spanning parallelograms with $|\det| > 1$, or tilted to a non-nearest-neighbour angle. Four families are compared on the licensed sheet — the axis rectangle $(1, 0)/(0, 1)$, a determinant-one loop tilted to $(1, 1)/(0, 1)$, the diamond $(1, 1)/(1, -1)$ with $\det = 2$, and a third angle $(2, 1)/(-1, 1)$ with $\det = 3$ — each measured for its exact minimum surface area, its flip-sector degeneracy N_{sector}, and its Creutz tension. Three results hold to numerical precision through $R, T \leq 3$ for all four families (the entropy closed forms are further verified on square loops to $L = 5$ for the determinant-one families and $L = 4$ for the diamond; the determinant-three family is checked through $R, T \leq 3$, its $L = 4$ sector count exceeding the finite search horizon).

First, there is no undercut: the exact minimum area equals the flat reference area $4\det RT$ for every loop, so no tilted loop finds a shorter surface through the bulk. Second, because the area is exactly $4\det RT$, the Creutz mixed difference gives

$$\chi_{\text{area}} = 4\det\,\sigma, \qquad \frac{\chi_{\text{area}}}{4\det} = \sigma = -\log(\beta/18),$$

identical across all four families with zero spread: the bare string tension is isotropic beyond the primitive directions. Third, the flip-sector degeneracy follows an exact closed form,

$$N_{\text{sector}} = 2^{(R-1)(T-1)}, \quad 2^{(R-1)(T-2)}, \quad 2^{(2R-1)(T-1)}, \quad 2^{(3R-1)(T-1)}$$

for the four families respectively. Each exponent has leading term $\det\cdot RT$, the cell count, so the entropy density $\log_2 N_{\text{sector}}/(\text{cells}) \to 1$ bit per cell for every orientation and non-primitivity. The *bulk* roughening entropy is therefore isotropic; the orientation dependence is confined to the subleading term, which tracks the loop perimeter and vanishes per unit area as the loop grows.

Both the bare tension and the bulk roughening-entropy density therefore stay controlled and isotropic beyond primitive rhombi. This remains finite and leading-order — weak-coupling scaling and continuum $SO(3)$ are still open — but the nonprimitive-direction and off-axis-entropy questions are now settled at the same order as the primitive gate.

7 The bulk baryon Y-string

7.1 The gauge-invariant baryon operator

The closed-cell triality theorem says that a qqq source is allowed. The bulk string calculation asks how it is represented dynamically. The natural gauge-invariant operator has three Wilson arms meeting at one ϵ-junction:

$$B = \epsilon_{abc}\, U_1{}^{a}{}_{a'} U_2{}^{b}{}_{b'} U_3{}^{c}{}_{c'}\, q_1^{a'} q_2^{b'} q_3^{c'}.$$

Under a common gauge rotation $g \in \mathrm{SU}(3)$ at the junction,

$$\epsilon_{abc} g^{a}{}_{i} g^{b}{}_{j} g^{c}{}_{k} = (\det g)\epsilon_{ijk} = \epsilon_{ijk}.$$

Thus the junction is not an extra fitted object; it is the standard SU(3) invariant tensor.

7.2 Exact finite Steiner problem

The geometry problem is the three-terminal Steiner problem (find the junction minimizing the total length of three arms reaching the three sources) on the same bond graph used for the finite bulk. For the tri-axial source family

$$J = (1,1,1), \qquad q_1 = J + n\hat{x}, \quad q_2 = J + n\hat{y}, \quad q_3 = J + n\hat{z},$$

the exact graph distances are

$$d(q_1, q_2) = d(q_2, q_3) = d(q_3, q_1) = 2n.$$

The matched meson length is therefore

$$L_M = d(q_1, q_2) = 2n.$$

The exact three-terminal minimum is

$$L_Y = \min_{J'}\{d(q_1, J') + d(q_2, J') + d(q_3, J')\} = 3n,$$

with the original junction J as the witness. The executable check verifies this for $n = 1, \ldots, 4$.

At leading strong coupling, in the same normalization as the edge-loop observable,

$$V_M = 4\sigma L_M, \qquad V_B = 4\sigma L_Y.$$

Consequently, for this equal-arm finite slice,

$$\frac{V_B}{V_M} = \frac{L_Y}{L_M} = \frac{3}{2}.$$

Remark 2. *The* $3/2$ *is not a universal meson:baryon mass ratio. It is the ratio for one matched tri-axial source family: three baryon arms of length* n *versus one meson line of length* $2n$*. The robust physical result is the* Y*-law and the universality of* σ*, not the numerical ratio divorced from this geometry.*

7.3 Relation to lattice-QCD baryon potentials

Lattice studies of the static three-quark potential find that, at large distance, the baryonic flux is well described by a Y-ansatz: a minimal connected flux network with a universal string tension, plus Coulomb and constant terms [9–11]. The finite result here has the same structural form:

$$V_{3Q} \sim \sigma L_{\min} + \cdots .$$

It does not compute the continuum value of σ, the Coulomb coefficient, the Luescher term [12], or spin/flavour spectroscopy. It shows that the finite record geometry supports the correct kind of baryonic colour operator: a single gauge-invariant ϵ-junction with three flux arms and the same string tension per unit length as the meson.

There is one caveat to state plainly. In the axis-aligned graph metric used for the executable tri-axial family,

$$\frac{1}{2}\left[d(q_1, q_2) + d(q_2, q_3) + d(q_3, q_1)\right] = 3n = L_Y.$$

The follow-up off-axis audit shows this is not an accident of the tri-axial family. The present finite bond graph is a cubic-grid median graph, and for any three terminals in such a metric

$$L_Y(q_1, q_2, q_3) = \frac{1}{2}\left[d(q_1, q_2) + d(q_2, q_3) + d(q_3, q_1)\right].$$

The script exhaustively checks all 317,750 triples in a 5^3 box, including 315,892 non-collinear off-axis triples and 6,940 graph-equilateral triples, and finds no separation. Thus no larger finite off-axis search in this metric can distinguish a continuum Y-ansatz from a half-perimeter Δ-ansatz by length alone. The Y character in this finite gate comes from the ϵ-junction operator. A geometric Y-versus-Δ separation requires an effective Euclidean or weak-coupling flux metric, off-graph interpolation, or a continuum baryonic-potential calculation.

8 Finite-temperature deconfinement

Everything above is a zero-temperature, static statement: it prices a fixed colour source by the minimal area its Wilson surface spans. Confinement, however, is the low-temperature phase of a system that *deconfines* when heated, and that transition has its own order parameter — the Polyakov line — which none of the previous rungs could see. A Polyakov line wraps a non-contractible Euclidean-time cycle. On a contractible loop the single-link centre average vanishes identically,

$$\int_{\mathrm{SU}(3)} U \, dU = 0,$$

so a contractible "Polyakov" average merely re-expresses the closed-cell triality selection of Section 3; it carries no thermodynamic information. The genuine order parameter needs two ingredients the static calculation lacks: a periodic thermal time direction, giving the loop something non-contractible to wrap, and a centre-symmetric action that can break *spontaneously*. This section supplies both and follows the resulting transition from a standard lattice, where it can be checked against known values, onto the framework's own bulk.

8.1 The Polyakov order parameter

Give the complex a periodic Euclidean-time direction of extent N_t, with a gauge link on every spatial edge in each time slice and a time-link on every spatial vertex. The volume-averaged Polyakov line is

$$L = \frac{1}{N_v} \sum_v \frac{1}{3} \operatorname{Tr} \prod_{t=0}^{N_t-1} U_{\text{time}}(v,t),$$

replaced for the Z_3 centre theory by the phase $L = \frac{1}{N_v} \sum_v \omega^{\sum_t k_{\text{time}}(v,t)}$ with $\omega = e^{2\pi i/3}$. In the confined phase the centre symmetry is unbroken and, on a finite volume, $\langle |L| \rangle$ sits on the statistical floor $\sim 1/\sqrt{N_v}$; in the deconfined phase the centre breaks and $\langle |L| \rangle = O(1)$. The transition exists only beyond the leading strong coupling used by every earlier rung, so it is located here by direct Monte Carlo: a vectorised checkerboard Metropolis sampling of the Wilson action $S = -(\beta/N) \sum_p \Re \operatorname{Tr} U_p$, with the susceptibility $\chi = N_v \operatorname{Var}(|L|)$ peaking at the critical coupling β_c.

8.2 A five-step validation arc

The order parameter is assembled in five steps (Table 1, Fig. 2), deliberately ordered so that the framework-specific result is reached only after the machinery has been validated against known lattice numbers.

1. Z_3 **on a hypercubic torus.** The centre group — the symmetry that governs SU(3) deconfinement — on a standard four-dimensional lattice. $\langle |L| \rangle$ melts from the floor to ~ 1 with a susceptibility peak, giving the first genuinely *breakable* order parameter in the programme (every prior rung sat at a coupling where the transition cannot occur).

2. SU(3) **on a hypercubic torus.** The full gauge group, sampled with an $\exp(i \sum_a \theta_a \lambda_a)$ proposal and cold-start annealing. The half-plateau crossing gives $\beta_c = 5.06$ at $N_t = 2$ and $\beta_c = 5.72$ at $N_t = 4$; the latter reproduces the established lattice value 5.6925(2) [13], and the rise with N_t is the correct finite-temperature scaling. This is the quantitative validation of the machinery (the strong-coupling plaquette also equals $\beta/18$ exactly).

3. Z_3 **on the bond-bipyramid bulk.** The same centre theory on the framework's own geometry, with the spatial-face plaquettes and time-plaquettes built directly from the licensed complex. It deconfines, with β_c rising with N_t ($0.64 \to 0.73$).

4. SU(3) **on the bond-bipyramid bulk.** The full gauge group on the framework geometry. The technical step is the ordered matrix staple on an irregular complex — no shift-invariant stencil exists, so each link's staple is assembled from its loop-ordered plaquette partners — and the links stay in SU(3) to 10^{-14}. It deconfines, again with β_c rising with N_t ($\approx 4.3 \to 6.5$), at framework-specific couplings: *not* the hypercubic values, because the spatial faces are triangular and the action normalisation differs.

5. **Finite-size scaling to a precision coupling**, treated next.

Geometry	Gauge	N_t	β_c	Reading
hypercubic torus	Z_3	2	0.67	first breakable order parameter
hypercubic torus	SU(3)	2	5.06	early value ≈ 5.1
hypercubic torus	SU(3)	4	5.72	matches 5.6925(2) [13]
bond-bipyramid bulk	Z_3	2	0.64	framework deconfines
bond-bipyramid bulk	Z_3	4	0.73	correct N_t scaling
bond-bipyramid bulk	SU(3)	2	≈ 4.3	full group on framework
bond-bipyramid bulk	SU(3)	4	≈ 6.5	correct N_t scaling
bond-bipyramid (FSS)	Z_3	2	0.550	precision, $V \to \infty$

Table 1: Deconfinement critical couplings across the five steps. The two hypercubic SU(3) rows are the validation against known lattice values; the bond-bipyramid rows are framework-specific. Couplings are lattice-unit β in the Wilson normalisation $S = -(\beta/N)\sum_p \Re\,\mathrm{Tr}\,U_p$ ($N = 3$ for SU(3); the Z_3 centre uses $S = -\beta\sum_p \cos(2\pi E_p/3)$), so the Z_3 and SU(3) columns are on different scales and are not directly comparable.

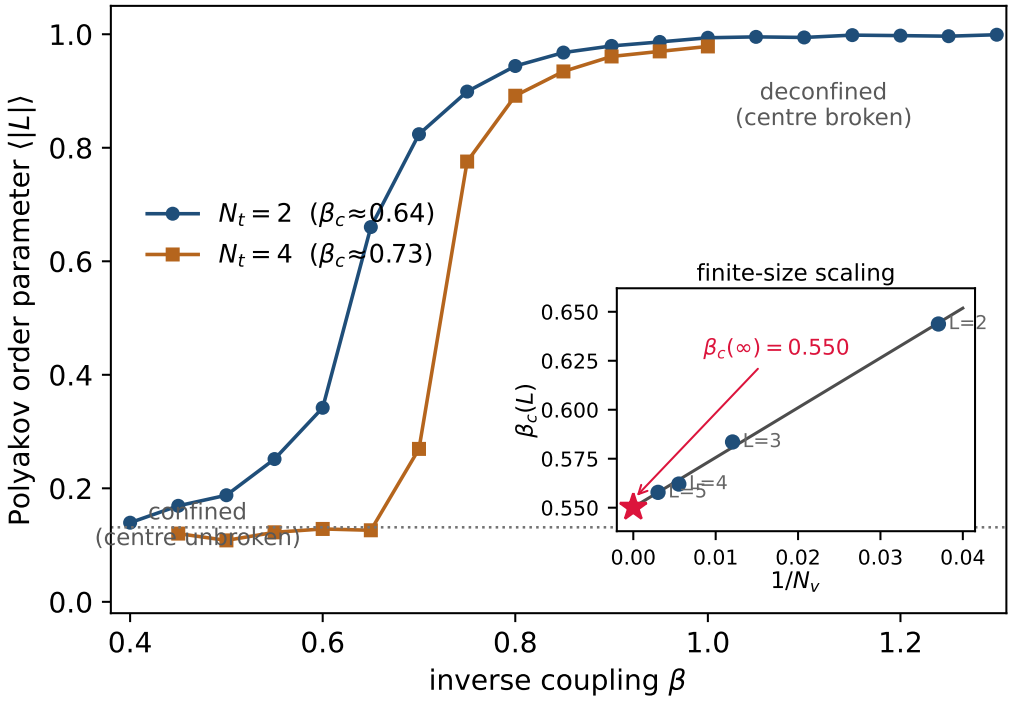

Figure 2: Finite-temperature deconfinement on the bond-bipyramid TCH bulk. Main panel: the Z_3 Polyakov order parameter $\langle|L|\rangle$ melts from the finite-size floor (confined, centre unbroken) to $O(1)$ (deconfined, centre broken) as the inverse coupling β grows, with the transition moving to larger β as the thermal extent N_t increases — the finite-temperature scaling. Inset: finite-size scaling of the critical coupling $\beta_c(L)$, read from the susceptibility peak on cubic slabs $L = 2, 3, 4, 5$ (spatial volumes $N_v = 27, 83, 181, 333$); it is linear in $1/N_v$ and extrapolates to $\beta_c(\infty) = 0.550$ (star).

8.3 Finite-size scaling and a precision coupling

The bulk couplings in steps three and four are single-volume measurements, and a single small volume systematically *overestimates* β_c. The finite-size-scaling step removes that bias for the cheap Z_3 centre theory; the identical procedure applies to SU(3) at higher cost. Running the bulk transition on cubic slabs $L = 2, 3, 4, 5$ (spatial volumes $N_v = 27, 83, 181, 333$) and locating $\beta_c(L)$ by a parabolic fit to the susceptibility peak gives a clean linear convergence in the inverse volume,

$$\beta_c(L) = \beta_c(\infty) + \frac{a}{N_v}, \qquad \beta_c(\infty) = 0.550, \quad a \approx 2.54,$$

with a maximum fit residual of 0.003 (Fig. 2, inset). Two independent signatures confirm a genuine transition rather than a crossover: the susceptibility peak *grows* with volume ($\chi_{\max} = 0.95, 2.33, 2.89, 3.50$), and $\beta_c(L)$ drifts monotonically and converges. The single-volume demonstration value (0.64) is thus a finite-size artefact; the infinite-volume bulk coupling 0.550 sits *below* the hypercubic Z_3 value (≈ 0.67 in the same normalisation), a genuine framework feature — the bulk's higher plaquette-per-link connectivity makes it deconfine more readily.

Remark 3. *This section is demonstration-grade: small slabs and modest statistics. The* SU(3) *bulk couplings are located to about* ± 0.2*, not lattice precision; the finite-size scaling pins the* Z_3 *bulk coupling but not the* order *of the transition, which would require Binder cumulants and more volumes; and the framework* β_c *values are specific to the bond-bipyramid geometry and action normalisation, so they are not, and must not be read as, the hypercubic numbers. What the section establishes is structural and now end-to-end: the framework carries a genuine, breakable deconfinement order parameter with the correct finite-temperature* N_t *scaling, validated against a known lattice value before being measured — for both the centre and the full gauge group — on its own geometry.*

9 Executable audit trail

Table 2 lists the scripts used by the paper. They are small finite regression tests. An exit code of zero means the stated identities passed.

10 Status and frontiers

The finite confinement ladder now has several distinct tiers.

The two most natural next calculations are therefore not needed for this paper, but they are clear:

1. **Physical string tension.** The present $\sigma = -\log(\beta/18)$ is only the leading strong-coupling lattice-unit coefficient. The scale-setting audit shows that it fails the current $T_c/\sqrt{\sigma}$ constancy check. The next real rung is a full SU(3) bulk production scaling run measuring both $\beta_c(N_t)$ and $a\sqrt{\sigma}(\beta)$ on larger volumes and larger Wilson loops. The ordinary cubic Cornell extractor is now validated, but the matched TCH straight-path and first variational operators are not scale-setting on the present slabs. The observed $\beta/3$ two-point normalization lead is not yet a theorem.

2. **Continuum baryon geometry.** The finite bond graph has now been checked: off-axis and graph-equilateral source families still obey $L_Y = \frac{1}{2}P$. A true Y-versus-Δ length separation therefore requires a weak-coupling or effective Euclidean flux metric, not a larger finite-graph search.

3. **Full-slab roughening entropy.** Extend the tight-strip transfer theorem to wider-margin surfaces, measuring the thick-string entropy density rather than assuming it.

Script	Purpose
`record_grammar_tch_colour_singlet_gauss.py`	Closed-shell $\mathbb{F}_3$ Gauss law; lone fundamental forbidden; $q\bar{q}$ and $qqq\epsilon$ admitted.
`record_grammar_tch_bond_bipyramid_bulk.py`	Corrected bond-centred bipyramid sheets and slabs; finite 3-ball topology gate; small-surface ledger check.
`record_grammar_tch_bulk_block_static_potential.py`	Negative topology gate for the naive corner-stacked block; prevents a false static-potential extraction.
`record_grammar_tch_bond_bipyramid_isoperimetry.py`	Licenses flat offset sheets; retires the $P = 2A$ family.
`record_grammar_tch_bond_bipyramid_edge_loop_creutz.py`	Edge-loop Wilson family; $A_{\mathrm{ref}} = 4RT$, $P = 4(R+T) - 2$, Creutz separation.
`record_grammar_tch_string_tension_continuum_scaling_audit.py`	Physical-σ scale-setting audit; shows the strong-coupling coefficient fails $T_c/\sqrt{\sigma}$ constancy and records $\beta_{\mathrm{eff}} = \beta/3$ only as a candidate normalization lead.
`record_grammar_tch_su3_bulk_scale_setting.py`	First full-SU(3) bulk scale-setting harness; measures Polyakov susceptibility and 1×1 Creutz ratios on the same ensembles. Local profile verdict: not scale-set.
`record_grammar_tch_su3_scaling_gate.py`	Conservative post-processor for scale-setting runs; tests whether $T_c/\sqrt{\sigma}$ stabilizes across N_t, finite volume, and sigma-estimator quality before any physical string tension is promoted.
`record_grammar_cubic_su3_static_potential_pipeline.py`	Ordinary hypercubic Wilson-SU(3) zero-temperature static-potential control. With smearing and a Cornell fit it validates the extractor at demonstration grade ($T_c/\sqrt{\sigma} \simeq 0.645$ at smear 4).
`record_grammar_tch_su3_static_potential_pipeline.py`	Ports the same Cornell readout to straight-path bond-bipyramid operators; current blocks give negative σ, identifying a TCH geometry/operator/volume limitation.
`record_grammar_tch_su3_variational_static_potential.py`	First geometry-specific TCH variational source basis. Positive small-R diagnostics but no stable Cornell scale setting yet; $R = 4$ still lacks detour support on the present slab.
`record_grammar_tch_bond_bipyramid_transfer_matrix.py`	Exact tight-strip transfer count; $N_{\min} = 2^{(R-1)(T-1)}$, $D_R = 2^{R-1}$.
`record_grammar_tch_bond_bipyramid_isotropy.py`	Finite cubic-axis/in-sheet isotropy gate for the edge-loop Creutz observable.
`record_grammar_tch_bond_bipyramid_offaxis_isotropy.py`	Primitive off-axis Wilson-rhombus isotropy gate on the triangular sheet; $\Delta\chi_{\mathrm{area}} = 3.2 \times 10^{-14}$.
`record_grammar_tch_bond_bipyramid_nonprimitive_isotropy.py`	Non-primitive/tilted Wilson loops; no undercut, $\chi_{\mathrm{area}}/(4\det) = \sigma$, exact N_{sector} forms with bulk entropy density 1 bit/cell.
`record_grammar_tch_bond_bipyramid_baryon_y_string.py`	Bulk $qqq\epsilon$ baryon Y-string versus matched meson string; $L_Y = 3n$, $L_M = 2n$.
`record_grammar_tch_bond_bipyramid_baryon_offaxis_delta_audit.py`	Off-axis/equilateral baryon Y-versus-Δ audit; proves the present median graph forces $L_Y = \frac{1}{2}P$ for every three-source family.
`record_grammar_tch_z3_polyakov_torus.py`	Finite-T Z_3 Polyakov order parameter on a hypercubic torus; first breakable order parameter.
`record_grammar_tch_su3_polyakov_torus.py`	SU(3) deconfinement and β_c-vs-N_t scaling; $\beta_c(N_t{=}4) = 5.72$ versus lattice 5.6925(2).
`record_grammar_tch_bulk_polyakov_torus.py`	Z_3 deconfinement on the bond-bipyramid bulk $\times$ periodic time; $\beta_c(N_t) = 0.64/0.73$.
`record_grammar_tch_su3_bulk_polyakov_torus.py`	Full SU(3) on the bulk (ordered staple on the irregular complex); $\beta_c(N_t) \approx 4.3/6.5$.
`record_grammar_tch_fss_betac.py`	Finite-size scaling of the bulk β_c on cubic slabs; $\beta_c(\infty) = 0.550$.

Table 2: Executable audit trail for the finite confinement ladder. The public code repository is [14].

Claim	Status	What remains
Closed-cell singlet selection	Exact finite theorem	None at centre-triality level; full spectroscopy is separate.
Corrected bulk geometry	Structural finite result	Continuum embedding and larger periodic/thermal complexes.
Wilson edge-loop string tension	Leading strong-coupling finite result	Physical σ needs full SU(3) bulk scale setting: $a\sqrt{\sigma}(\beta)$, $\beta_c(N_t)$, and a derived β normalization.
Transfer ledger	Exact tight-strip theorem	Wider-margin/full-slab roughening entropy.
Cubic-axis, primitive and non-primitive isotropy	Finite gate (tension + entropy)	Continuum $SO(3)$, weak-coupling scaling.
Baryon Y-string	Finite graph result plus finite-graph $Y = \Delta$ no-go	Weak-coupling/continuum baryon potentials, Coulomb/Luescher terms, spin/flavour structure, proton mass.
Finite-T order parameter	Monte Carlo, validated vs lattice	Continuum T_c, order of the transition (Binder cumulants).
Deconfinement on the bulk	Finite framework result	SU(3) precision, full finite-size scaling, continuum limit.

Table 3: What is closed and what is not. The paper's claims are finite and leading-order unless explicitly labelled exact.

11 Conclusion

The finite-QEC record grammar now gives a compact confinement story with a clear division of labour. Closed-cell Gauss law forbids net triality. The corrected bond-bipyramid bulk licenses finite Wilson surfaces. The leading strong-coupling Wilson action gives a string tension. The transfer theorem measures the worldsheet entropy and places the ledger in a two-dimensional tensor-network class. The isotropy gates show the finite observable is independent across the tested cubic-axis and primitive off-axis directions. The baryon calculation places the proton colour sector in the bulk as a genuine $qqq\epsilon$ Steiner-Y record, while the off-axis audit proves that the current median graph cannot separate Y from Δ by length alone. Finally, a finite-temperature section closes the loop: a Monte Carlo Polyakov-loop order parameter, validated against the known SU(3) deconfinement coupling and then measured on the framework's own bulk for both the Z_3 centre and the full gauge group, with a finite-size-scaled critical coupling.

The result is not continuum QCD. It is a finite, reproducible strong-sector certificate. That is its value. It shows that the framework's colour sector does not merely name the proton as a singlet; it builds the allowed singlet, prices its Wilson strings with the same tension as mesons, and exposes the ledger complexity that must be carried by the record algebra.

Acknowledgement

The author thanks the ongoing Codex-assisted audit process for executable checks, negative controls, and repeated pressure to separate finite theorems from continuum claims.

References

[1] Kenneth G. Wilson. Confinement of quarks. *Physical Review D*, 10(8):2445–2459, 1974. doi: 10.1103/PhysRevD.10.2445.

[2] John Kogut and Leonard Susskind. Hamiltonian formulation of Wilson's lattice gauge theories. *Physical Review D*, 11(2):395–408, 1975. doi: 10.1103/PhysRevD.11.395.

[3] John B. Kogut. An introduction to lattice gauge theory and spin systems. *Reviews of Modern Physics*, 51(4):659–713, 1979. doi: 10.1103/RevModPhys.51.659.

[4] David Elliman. An executable record grammar for quantum correlations. https://doi.org/10.5281/zenodo.21034325, 2026. Concept and executable finite record-grammar paper.

[5] Heinz J. Rothe. *Lattice Gauge Theories: An Introduction*. World Scientific, 4 edition, 2012. doi: 10.1142/8229.

[6] Michael Creutz. Monte carlo study of quantized SU(2) gauge theory. *Physical Review D*, 21 (8):2308–2315, 1980. doi: 10.1103/PhysRevD.21.2308.

[7] F. Verstraete, V. Murg, and J. I. Cirac. Matrix product states, projected entangled pair states, and variational renormalization group methods for quantum spin systems. *Advances in Physics*, 57(2):143–224, 2008. doi: 10.1080/14789940801912366.

[8] Román Orús. A practical introduction to tensor networks: Matrix product states and projected entangled pair states. *Annals of Physics*, 349:117–158, 2014. doi: 10.1016/j.aop.2014.06.013.

[9] T. T. Takahashi, H. Suganuma, Y. Nemoto, and H. Matsufuru. Detailed analysis of the three-quark potential in SU(3) lattice QCD. *Physical Review D*, 65(11):114509, 2002. doi: 10.1103/PhysRevD.65.114509.

[10] Gunnar S. Bali. QCD forces and heavy quark bound states. *Physics Reports*, 343(1):1–136, 2001. doi: 10.1016/S0370-1573(00)00079-X.

[11] F. Okiharu, H. Suganuma, and T. T. Takahashi. Detailed analysis of the tetraquark potential and flip-flop in SU(3) lattice QCD. *Physical Review D*, 72(1):014505, 2005. doi: 10.1103/PhysRevD.72.014505.

[12] M. Lüscher. Symmetry-breaking aspects of the roughening transition in gauge theories. *Nuclear Physics B*, 180(2):317–329, 1981. doi: 10.1016/0550-3213(81)90423-5.

[13] G. Boyd, J. Engels, F. Karsch, E. Laermann, C. Legeland, M. Lütgemeier, and B. Petersson. Thermodynamics of SU(3) lattice gauge theory. *Nuclear Physics B*, 469(3):419–444, 1996. doi: 10.1016/0550-3213(96)00170-8.

[14] David Elliman. It-from-bit model: public executable scripts. https://github.com/dgedge/itfrombit, 2026. Repository containing public code artifacts associated with the finite-QEC record-grammar programme.

[15] Reinhard Diestel. *Graph Theory*. Springer, 5 edition, 2017. doi: 10.1007/978-3-662-53622-3.

A Derivation details

A.1 Connected-graph incidence rank over $\mathbb{F}_3$

For a connected graph with $|V|$ vertices, the oriented incidence matrix has one row dependency: the sum of all rows is zero. Removing any one row leaves a matrix of rank $|V| - 1$, because a spanning tree already has incidence rank $|V| - 1$ [15]. Therefore

$$\operatorname{rank} B = |V| - 1.$$

The image of B is contained in

$$H = \left\{ x \in \mathbb{F}_3^V : \sum_v x_v = 0 \right\},$$

and $\dim H = |V| - 1$. Hence $\operatorname{im} B = H$. This is the whole closed-cell triality theorem.

A.2 Strong-coupling coefficient

For the Wilson plaquette action, the leading nontrivial insertion in the fundamental character expansion contributes one fundamental plaquette factor per spanning face. In the normalization used here,

$$u_F = \frac{\beta}{2N^2} = \frac{\beta}{18}, \qquad N = 3.$$

A minimum surface with A triangular face units contributes

$$u_F^A = \exp[-A \log(18/\beta)].$$

Thus the lattice-unit string tension per face unit is

$$\sigma = -\log u_F = -\log(\beta/18).$$

The edge-loop family used in this paper has four triangular face units per spatial graph step, giving 4σ per graph edge in the static-potential normalization.

A.3 Creutz cancellation

Let

$$Y(R,T) = \sigma\, 4RT + \mu\,[4(R+T) - 2] + c.$$

The mixed difference

$$\Delta_R \Delta_T Y = Y(R,T) + Y(R+1,T+1) - Y(R+1,T) - Y(R,T+1)$$

gives

$$\Delta_R \Delta_T (4\sigma RT) = 4\sigma, \qquad \Delta_R \Delta_T [4\mu(R+T) - 2\mu] = 0, \qquad \Delta_R \Delta_T c = 0.$$

Thus the Creutz ratio isolates the area coefficient only after a loop family with independent area and perimeter has been licensed.

A.4 Baryon Steiner length on the tri-axial graph

In the cubic bond graph, let

$$J = (1,1,1), \qquad q_i = J + n\hat{e}_i.$$

The graph distance is Manhattan distance, so

$$d(q_i, q_j) = 2n \quad (i \neq j).$$

For any candidate junction J', the sum

$$S(J') = \sum_i d(q_i, J')$$

is minimized coordinatewise by any median of the three source coordinates. For the tri-axial family, the coordinatewise median is exactly J. Hence

$$\min_{J'} S(J') = S(J) = n + n + n = 3n.$$

The executable script verifies the same result by an exact three-terminal Steiner dynamic programme on the finite bond graph.